CHEMISTRY
AN ASIAN JOURNAL
www.chemasianj.org

Accepted Article

Title: Cancer-Cell Imaging Using Copper-Doped Zeolite Imidazole Framework-8 Nanocrystals Exhibiting Oxidative Catalytic Activity

Authors: Changjoon Keum, Sangwoo Park, and Sang-Yup Lee

To be cited as: *Chem. Asian J.* 10.1002/asia.201800749

Link to VoR: http://dx.doi.org/10.1002/asia.201800749

A Journal of
ACES Asian Chemical Editorial Society

A sister journal of Angewandte Chemie and Chemistry – A European Journal

WILEY-VCH

Cancer-Cell Imaging Using Copper-Doped Zeolite Imidazole Framework-8 Nanocrystals Exhibiting Oxidative Catalytic Activity

Changjoon Keum,[†, a] Sangwoo Park,[†, b] and Sang-Yup Lee*[, a]

Abstract: Copper-doped zeolite imidazole framework-8 (Cu/ZIF-8) is prepared and its peroxidase-like oxidative catalytic activity is examined with a demonstration of its applicability for cancer cell imaging. Through simple solution chemistry at room temperature, Cu/ZIF-8 nanocrystals are produced that catalytically oxidize an organic substrate of *o*-phenylenediamine in the presence of H_2O_2. In a similar manner to peroxidase, the Cu/ZIF-8 nanocrystals oxidize the substrate through a ping-pong mechanism with an activation energy of 59.2 kJ·mol^{-1}. The doped Cu atoms work as active sites in which the active Cu intermediates are expected to be generated during the catalysis, whereas the undoped ZIF-8 does not show any oxidative activity. Cu/ZIF-8 nanocrystals exhibit low cell toxicity and display catalytic activity through interaction with H_2O_2 among various reactive oxygen species in a cancer cell. This oxidative activity *in vitro* allowed cancer-cell imaging exploiting the photoluminescence emitted from the oxidized product of *o*-phenylenediamine, which was insignificant in the absence of the Cu/ZIF-8 nanocrystals. The results of this study imply that the Cu/ZIF-8 nanocrystal is a promising catalyst for the analysis of the microbiological systems.

Introduction

The zeolitic imidazolate framework (ZIF), a subclass of metal organic frameworks (MOFs), possesses zeolite topologies and general characteristics of MOFs, such as chemical and thermal stability, large surface area, unimodal porosity, and controllable chemical functionality.[1,2] Many ZIF materials have been explored because of their high potential in various applications as porous materials.[3–7] ZIF-8 is a subtype of ZIF materials whose ordered, porous structure was constructed through the assembly of Zn ions with 2-methylimidazole linkers. Recently, ZIF-8 has attracted research interest because of its ease of synthesis. Specifically, a water-based synthesis method reported by Lai et al. offers a facile way to prepare ZIF-8 while allowing designer modification.[8] According to this method, ZIF-8 nanocrystals on the order of tens of nanometres can be produced by mixing the Zn ion source and 2-methylimidazolate together at room temperature for several minutes. This water-based method surmounts the disadvantages of other methods, including the solvothermal,[9] microwave,[10,11] and sonochemical[12] approaches, where toxic organic solvents and other chemical additives were required with heat treatment (~200 °C).[13–15]

In addition to its mild synthesis conditions, ZIF-8 is advantageous for catalytic material preparation because of its high porosity and multiple sites to create active centres in the crystalline structure. By involving heterogeneous ionic or molecular species in ZIF-8, catalytic activity can be displayed from Zn ions through the synergetic effect of organic linker molecules. Although only a small number of studies have been reported, one simple way to afford catalytic activity is doping heterogeneous metal ions through which Zn ions are substituted with heterogeneous metal ions. In 2009, Schubert et al. prepared cobalt- or copper-doped bimetallic ZIF-1 ($Zn(im_2)_2$, im: imidazole) by acidic hydrothermal synthesis at 80–150 °C. Doping of these transition-metal ions to ZIF-1 resulted in the alteration of the crystalline structure and the expression of the paramagnetic property originating from the doped Co atoms.[16] Recently, catalytic applications of the metal-doped ZIF materials were also reported; the Cu-doped ZIF-8 (Cu/ZIF-8) exhibited catalytic activity for condensation reactions. The Cu^{2+} ions positioning randomly in ZIF functioned as Lewis acids in the Friedländer reaction to promote condensation of 2-aminobenzophenone and methylene.[17] Partial replacement of Zn with Fe ions in ZIF-8 was also applied for the catalysis of oxygen reduction in acidic solutions where imidazole-bonded Fe atoms, in the form of FeN_4, are likely to work as active sites for oxygen-reduction catalysis.[18] These reports imply that the metal-doped ZIF-8 can exhibit catalytic activity from the defects of the metal-imidazole complexes.

On the other hand, ZIF has been examined for drug delivery and bioimaging, exploiting its porous structure and structural sensitivity to the environmental changes. Delivery of anti-cancer drugs was performed using ZIF-8 as a porous host matrix in which drugs were highly loaded and then were released progressively by pH triggering.[19,20] Its sensitivity to cytoplasmic stimuli makes ZIF promising for a drug carrier accessible to the target cell. In a similar fashion, cell imaging was achieved by releasing fluorescent dye in response to the metabolic products. Mao et al. reported imaging of the dynamics of the mitochondrial ATP in live cells with the use of a ZIF-90 enclosing rhodamine B. The mitochondrial ATP has higher coordination affinity than imidazole-2-carboxyaldehyde, a linker of ZIF-90, to collapse the ZIF-90 framework, resulting in the release of fluorescent dye.[21] Release of the fluorescent dye could also be achieved by a pH stimulus when ZIF-8 was adopted as a cargo of the fluorescent molecules.[22] The outcomes of these biomedical applications along with the low toxicity and stability in neutral solution would open the possibility of further use of ZIF-8 for other biological applications.

In this study, the Cu-doped ZIF-8 (Cu/ZIF-8) was demonstrated as a peroxidase-like catalyst exhibiting oxidative catalytic activity and was exploited for cancer-cell imaging through the interaction with reactive oxidative species (ROS) in

[a] Changjoon Keum and Prof. Sang-Yup Lee
Department of Chemical and Biomolecular Engineering, Yonsei University
50 Yonsei-ro, Seodaemun-gu, Seoul, Korea 03722
E-mail: leessy@yonsei.ac.kr
[b] Sangwoo Park
Korea Basic Science Institute, Gwangju Center
77 Yongbong-ro, Buk-gu, Gwangju, Korea 61186
† Authors are equally contributed.

Supporting information for this article is given via a link at the end of the document.

the cell. Previously, biological cofactors were needed to display catalytic oxidative activity such that the well-known biological cofactor of hemin (or heme) has been involved in the MOF (including ZIF-8) through methods of cofactor solution wetting[23] or solvothermal synthesis[24–26]. These approaches utilized MOF materials as a simple support to which the heterogeneous species were implemented physically; thus, these hybrid MOFs had heterogeneous active sites and the chemical characteristics of ZIF materials were not extensively exploited for the expression of catalytic activity.[27] We report here that Cu/ZIF-8 exhibits catalytic oxidative activity by itself without other biological cofactors and that the catalytic activity of Cu/ZIF-8 with low toxicity can be exploited for the imaging of cancer cells. The catalytic activity of Cu/ZIF-8 was characterized and photoluminescence generated by the oxidation reaction in the target cell was visualized.

Results and Discussion

Characterization of Cu/ZIF-8

The Cu/ZIF-8 nanocrystals were prepared by mixing metal sources (Zn and Cu content: 90 and 10%, respectively) to the Hmim solution. The mixture solution became cloudy and finally formed a turbid suspension of Cu/ZIF-8 or ZIF-8 precipitates after 1 h of mixing. The obtained ZIF-8 and Cu/ZIF-8 were coloured white and beige, respectively. The colour change is

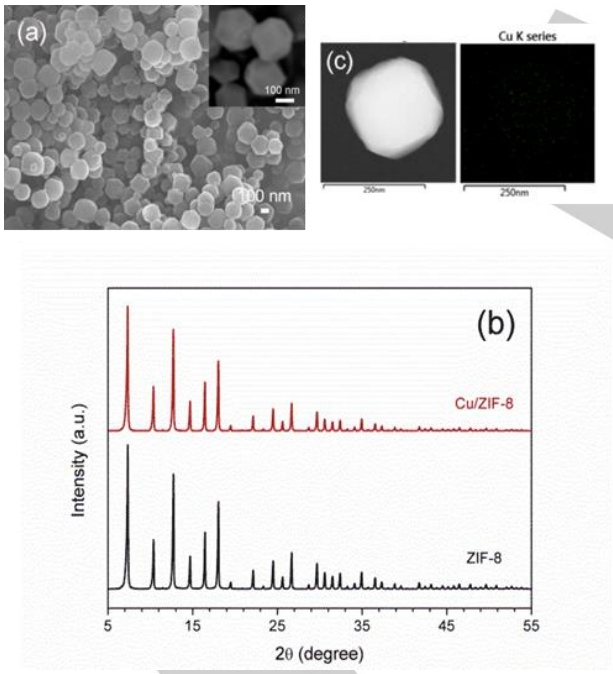

Figure 1. Shape and crystalline structure of Cu/ZIF-8. (a) SEM image of Cu/ZIF-8 (inset: magnified image of Cu/ZIF-8 showing dodecahedron structure), (b) X-ray diffraction spectra of ZIF-8 and Cu/ZIF-8, (c) Copper mapping on a Cu/ZIF-8 nanoparticle.

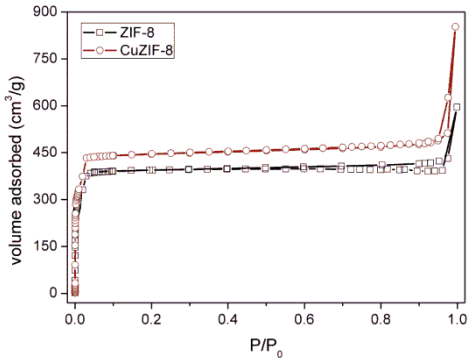

Figure 2. N_2 adsorption isotherm of Cu/ZIF-8 and ZIF-8 at 77 K.

indicative of Cu doping to ZIF-8.[17] The SEM images of Cu/ZIF-8 show that the synthesized nanocrystals have a rhombic dodecahedron structure, which is a typical morphology of ZIF-8 (Figure 1a).[28] The synthesized Cu/ZIF-8 has a diameter of 160 ± 47 nm which is slightly larger than that of ZIF-8 (151 nm). This slight increase of Cu/ZIF-8 is due to the retarded nucleation when Cu was added in the preparation of Cu/ZIF-8 crystals.[17] Except for a slight increase in size, no other morphology changes were observed after Cu doping compared to the intact ZIF-8. The powder X-ray diffraction (XRD) patterns of ZIF-8 and Cu/ZIF-8 also match each other, indicating little change in the crystal structure after Cu doping (Figure 1b). The invariance of the morphology and crystal structure indicates that doping with Cu ions does not significantly change the ZIF-8 crystalline structure. Doping of the Cu ions in Cu/ZIF-8 is confirmed from atomic mapping (Figure 1c).

The specific surface area and pore size of the Cu/ZIF-8 were evaluated from BET experiment. The N_2 adsorption/desorption curves at 77 K showed a reversible type-I isotherm (Figure 2).[5] This reversible type-I isotherm indicates that the prepared ZIFs have relatively small surface area and the N_2 adsorption is mostly determined by the accessible micropore volume, which is a general character of zeolites and MOFs.[28] It is likely that N_2 adsorbs on micropores at low pressure and on intrapores at high pressure. From the isotherm, the pore volume and pore size of ZIF-8 and Cu/ZIF-8 were determined, and are summarized in Table 1. The pore volume increased after Cu doping, presumably due to the generation of crystal defects and

Table 1. Porosity of Cu-doped/undoped ZIF-8

	ZIF-8	Cu/ZIF-8]
Pore volume (cc/g)	6.07×10^{-1}	6.85×10^{-1}
Pore size (Å)	6.38	6.28

the subsequent destruction of micropores by replacement of Zn with Cu.[29] The crystal defects may be caused by the difference in the coordination geometry of these two metal ions; Zn is tetrahedral and Cu is trigonal-pyramidal.[30] On the other hand, the pore size changed little (Δd = 1.6%), suggesting that the main frameworks of ZIF-8 were not considerably deformed.

The amount of the doped Cu in ZIF-8 was measured by inductively coupled plasma mass spectrometry (ICP-MS). The content of Cu in Cu/ZIF-8 was 5.1 wt%, which corresponds to the presence of 221 × 10^{-9} mol of Cu per 1 mg of Cu/ZIF-8. This small number explains the little change in XRD peaks after Cu doping; most of Cu/ZIF-8 keeps ZIF-8 framework even after doping of Cu.

Catalytic activity of Cu/ZIF-8

Doping of Cu to ZIF-8 partially replaces Zn ions to generate Cu-N_x complexes. This Cu–N_x generates vacancies[31] that may work as active sites for the oxidative catalysis. The oxidative catalytic activity from Cu/ZIF-8 was verified through a series of control experiments in which undoped ZIF-8 and other components for the catalysis were applied. For the catalytic activity test, 0.1 mg of Cu/ZIF-8 or ZIF-8 was dispersed in the 1.7 mL of OPD solution (10 mM) in HEPES buffer (50 mM, pH 7.2). Catalytic oxidation of OPD was initiated by the addition of 0.2 mL of H_2O_2, whose concentration became 2 mM in the reaction mixture. The linear increase in 2,3-diaminophenazine (DAP), the oxidized product of OPD, concentration was

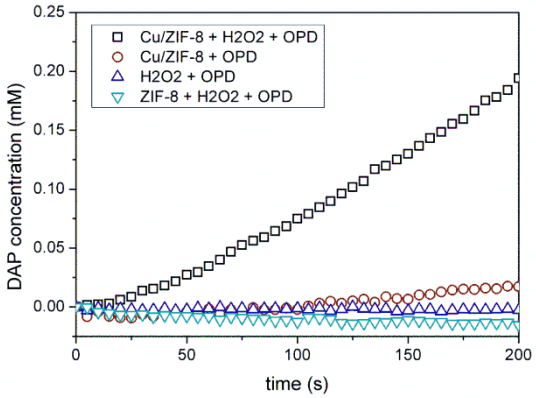

Figure 3. Profiles of the DAP produced by the catalytic function of Cu/ZIF-8.

observed only when Cu/ZIF-8 was added to the substrate mixture of OPD and H_2O_2 (Figure 3). In contrast, little production of DAP was observable when ZIF-8 was applied. This supports the idea that the doped Cu ions work as catalytic active sites while the Zn framework has little activity in itself. Catalytic oxidation in the presence of H_2O_2 proposes generation of the active Cu-peroxo intermediate species and subsequent oxidation occurs, like other catalysts containing copper center.[32,33] It is already known that the decomposition of H_2O_2 and the subsequent production of active metal-peroxo species

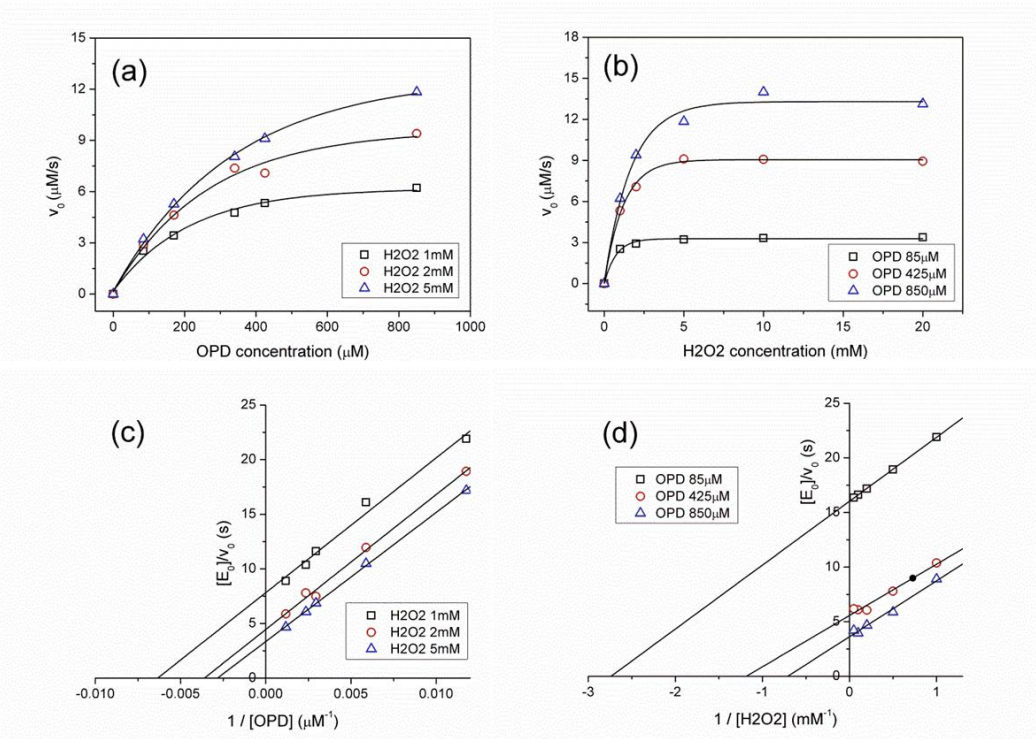

Figure 4. Apparent reaction rate profiles and double reciprocal plots of OPD oxidation by Cu/ZIF-8. The reaction kinetic assay was conducted based on the Michaelis-Menten kinetic model. The apparent reaction rate (v_0) and $[E_0]/v_0$ were plotted (a, c) for variable OPD concentrations at fixed concentrations of H_2O_2 (1, 2, and 5 mM), and (b, d) for variable H_2O_2 concentrations at fixed concentrations of OPD (85, 425, and 850 μM), respectively.

occur only when the metal atom is not fully coordinated with ligands.[31] Therefore, the imperfect coordination of Cu atoms to imidazoles in Cu/ZIF-8 nanocrystal presumably affords a free site for the coordination with H_2O_2, which leads to the expression of peroxidase-like activity.

The catalytic reaction mechanism was investigated from the plots of the apparent steady-state reaction rates that were measured with the variation in OPD and H_2O_2 substrate concentrations. The reaction rates (v_0) were determined from the slope of the linear DAP profiles at the early stage of reaction, wherein one substrate concentration varied while the other was fixed. The bi-substrate Michaelis–Menten kinetics model was applied to describe the reaction kinetics, like other peroxidase-like catalysts. The reaction rates of the oxidative catalysis fit well to the Michaelis–Menten kinetics model shown in Figure 4(a) and (b); the reaction rate linearly increased at low concentration and reached the maximum with the increase in the OPD and H_2O_2 concentrations. This Michaelis–Menten kinetics model indicates that the reaction rate is substrate-dependent and implies the generation of reactive intermediate species during the bi-substrate reaction.

Double-reciprocal plots were drawn to determine the bi-substrate kinetic parameters of the apparent turnover number (k_{cat}) and Michaelis constant (K_M). The parallel double-reciprocal plots were sketched with variation in both substrate concentrations (Figure 4c, d). The parallel double-reciprocal plots indicate that the Cu/ZIF-8 catalyst obeys the ping-pong mechanism that conveys the generation of catalytic intermediates by the association of the substrate to the catalytic active site. This ping-pong mechanism has generally been observed in other inorganic and organic peroxidase-mimetic catalysts wherein H_2O_2 works as the ROS to produce oxygen radicals.[28,34] The reaction rate (v_0) following the ping-pong mechanism can be presented by equation (1), and values of K_M and k_{cat} were calculated from the slope and y-intercepts. When calculating these kinetic parameters, the catalyst concentration [*Cata*] was set as the Cu concentration in Cu/ZIF-8 that was determined by ICP-MS mentioned above.

Table 2. Apparent kinetic parameters of Cu/ZIF-8 for catalytic OPD oxidation.

H_2O_2 concentration	k_{cat} (s^{-1})	K_M^{OPD} (mM)	k_{cat}/K_M^{OPD} ($M^{-1}s^{-1}$)
1 mM	0.128	0.158	810.6
2 mM	0.225	0.278	809.5
5 mM	0.299	0.353	845.8
OPD concentration	k_{cat} (s^{-1})	K_M^{H2O2} (mM)	k_{cat}/K_M^{H2O2} ($M^{-1}s^{-1}$)
85 μM	0.062	0.365	170.9
425 μM	0.180	0.845	212.8
850 μM	0.276	1.412	195.7

$$v_0 = \frac{k_{cat}\,[Cata][OPD][H_2O_2]}{K_M^{OPD}[H_2O_2] + K_M^{H_2O_2}[OPD] + [OPD][H_2O_2]} \quad (1)$$

The determined values of kinetic parameters, k_{cat} and K_M, are summarized in Table 2. Both k_{cat} and K_M increased with substrate concentration such that the catalytic efficiency (k_{cat}/K_M) did not change significantly with variation in the substrate concentrations. It is notable that K_M is much lower than that of other artificial peroxidase-like catalysts and comparable to that of natural HRP (see Table 3). Thus, Cu/ZIF-8 is inferred to have good affinity to the substrates even though it does not have other attracting/binding motifs for the substrates.

Table 3. k_{cat} and K_M values of peroxidase-like catalysts.

catalyst	substrate	k_{cat} (s^{-1})	K_M (mM)	Ref.
HRP	OPD	1.70 × 10-3	0.31	35
	H_2O_2	2.66 × 10-3	1.40	35
Cu_2O NWMCs	OPD	1.14 × 10-2	0.47	35
	H_2O_2	0.88 × 10-2	242	35
NDAus	OPD	290.4[a]	48.7	36
	H_2O_2	377.6[a]	208.7	36
Mn^{2+}-His bola	OPD	0.39	41.34	37
	H_2O_2	0.11	7.13	37
Cu/ZIF-8	OPD	0.13	0.16	this work
	H_2O_2	0.06	0.37	this work

[a] mM s^{-1} mg^{-2}

The catalytic property of Cu/ZIF-8 for OPD oxidation was further investigated in terms of the activation energy. The reaction rate (v_0) at the early stage of reaction was measured at various temperatures in the range of 30–50 °C. The reaction rate was assumed to be a pseudo-first-order reaction at the early stage of reaction, when the OPD concentration was excessive compared to the H_2O_2 concentration. The Arrhenius plot showing the linear correlation between the logarithm of the reaction rate constant (k) and inverse temperature (1/T) was drawn, and then the activation energy of 59.2 kJ·mol^{-1} was determined from the slope (Figure 5). This activation energy is comparable to that of other peroxidase-mimetic catalysts[35,36], but is still higher than that of graphene-based catalysts (20–28 kJ·mol^{-1})[37,38] and a natural peroxidase (27.1 kJ·mol^{-1}).[39] This relatively high activation energy is presumably due to the oxidation reaction of the active intermediate represented by the low turnover number rather than the binding affinity of the substrate to Cu/ZIF-8, considering the low values of K_M. The catalytic oxidation of OPD is influenced by the microenvironment around the active site wherein other oxygenated functional groups assist OPD oxidation.[40,41] Thus, absence of such oxygenated functional

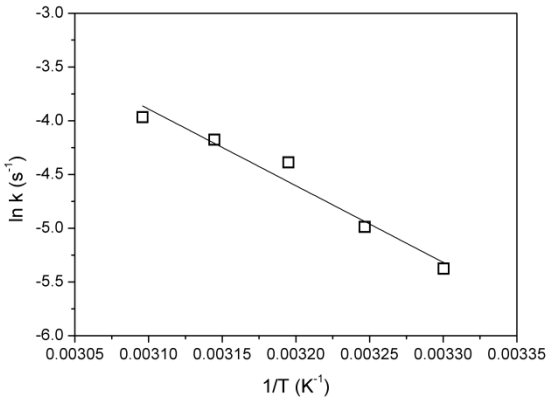

Figure 5. Arrhenius plot of Cu/ZIF-8 for the OPD oxidation in the temperature range of 30–50°C. Reaction rate k was determined from the slope of the DAP production profiles at the early stage of the catalysis. The reaction was assumed to be a first-order reaction.

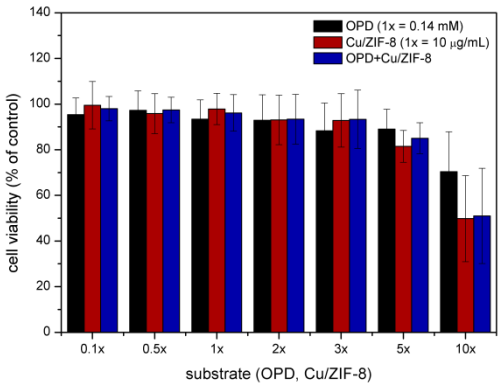

Figure 6. HeLa cell viability assay. HeLa cells were cultured in 96 well plate containing variable OPD or Cu/ZIF-8 concentrations for 12 h at 37°C. After incubation, MTT assay was performed and fluorescence intensity at 540 nm was read. Cells without addition of OPD or Cu/ZIF-8 were used as control.

group around the active Cu site of Cu/ZIF-8 is a potential factor for the high activation energy and low turnover number.

Cancer cell imaging by Cu/ZIF-8

Cancer cell imaging was demonstrated exploiting the catalytic activity of Cu/ZIF-8 with the ROS in a cell. Various ROS, like peroxide and hydroxyl radical (•OH), are generated as byproducts during the metabolism of oxygen in a cell[42] and can be utilized for the oxidative reaction of OPD or other organic dye in the presence of Cu/ZIF-8 catalyst. DAP, the oxidized form of OPD, emits green photoluminescence that can be used for cell imaging. Prior to conducting the cell imaging, the toxicity of Cu/ZIF-8 and OPD was examined using a HeLa cell line. Briefly, Cu/ZIF-8, OPD, and a mixture of these two at various concentrations were added to the HeLa cell suspension (1x corresponds to OPD = 0.14 mM and Cu/ZIF-8 = 10 μg/mL) in a 96-well plate and then incubated 12 h at 37 °C. After incubation, MTT assay was conducted to measure the cell viability. The HeLa cells showed good cell viability (average 92.7%) under exposure to 0.5x–5x of OPD (Figure 6). Because OPD is an aromatic diamine with low toxicity of median lethal dose (LD_{50}) of 44 mg/mL,[43] the high cell viability is reliable. In contrast, Cu/ZIF-8 showed considerable toxicity over 50 μg/mL (5x) concentration, although other studies reported low cytotoxicity of ZIF-8.[44] This low cell viability might come from the catalysed oxidation of cellular component by ROS in the presence of Cu/ZIF-8. Without the Cu/ZIF-8 catalyst, such significant oxidation would not occur; however, the presence of the catalyst promotes oxidation of cytoplasmic cellular components, resulting in a decrease in cell viability. The dissociated Cu species from the Cu/ZIF-8 also need to be counted, which may change the viability of the HeLa cell. We conducted ICP of the supernatant of the Cu/ZIF-8 suspension after 12 h incubation in pH 5.0 and 7.4 phosphate buffer solutions and found that 26.3 wt% and 18.4 wt% of Cu was liberated from Cu/ZIF-8, respectively (Supporting Information, Table S1). From the Cu release property, a dosage of 0.22 nM of copper ion per single HeLa cell was approximated. This amount of released Cu species is not critical to cause substantial cytotoxicity. The HeLa cell viability was higher than 90% at up to 5 μM of Cu ions, which was confirmed from a supplementary test (SI, Figure S1). This is in agreement with the reported critical concentration of 70 μM (=4.5 ppm) at which the cell viability is lower than 90%. [45]

Based on the results of cell viability test, HeLa cell imaging was conducted using Cu/ZIF-8 and OPD at concentrations of 30 μg/mL and 0.42 mM, respectively. Figure 7(a) shows the optical and confocal microscopy images of the cells. In the presence of both Cu/ZIF-8 and OPD, strong emission of the green photoluminescence was observable after 4 hours. The merged image confirms that the green fluorescence comes from the cell, not from the medium. In contrast, very weak green fluorescence was observable when OPD was solely applied without Cu/ZIF-8, and no fluorescence was emitted in the absence of OPD (data not shown). The fluorescence intensity was compared for the quantitative analysis of the effect of the Cu/ZIF-8 catalyst (Figure 7b). Around 2.5 times stronger fluorescence was observable when Cu/ZIF-8 was applied. This confocal microscopy analysis supports that OPD oxidation is promoted by Cu/ZIF-8 in the cell where the ROS are present.

As a control, the HEK293T cell line was tested for imaging through the same protocol. Optical and fluorescence microscopy images in Figure 7(c) show that little fluorescence was emitted from the HEK293T cells. This is probably because fewer ROS are present in the cytoplasm of the HEK293T cells, or less endocytosis of the OPD and Cu/ZIF-8 occurred. Although the clear reason for the weak fluorescence from HEK293T cell could not be rationalized, the control experiment supports that Cu/ZIF-8 can be exploited for cancer cell imaging where ROS are abundant to oxidize OPD.

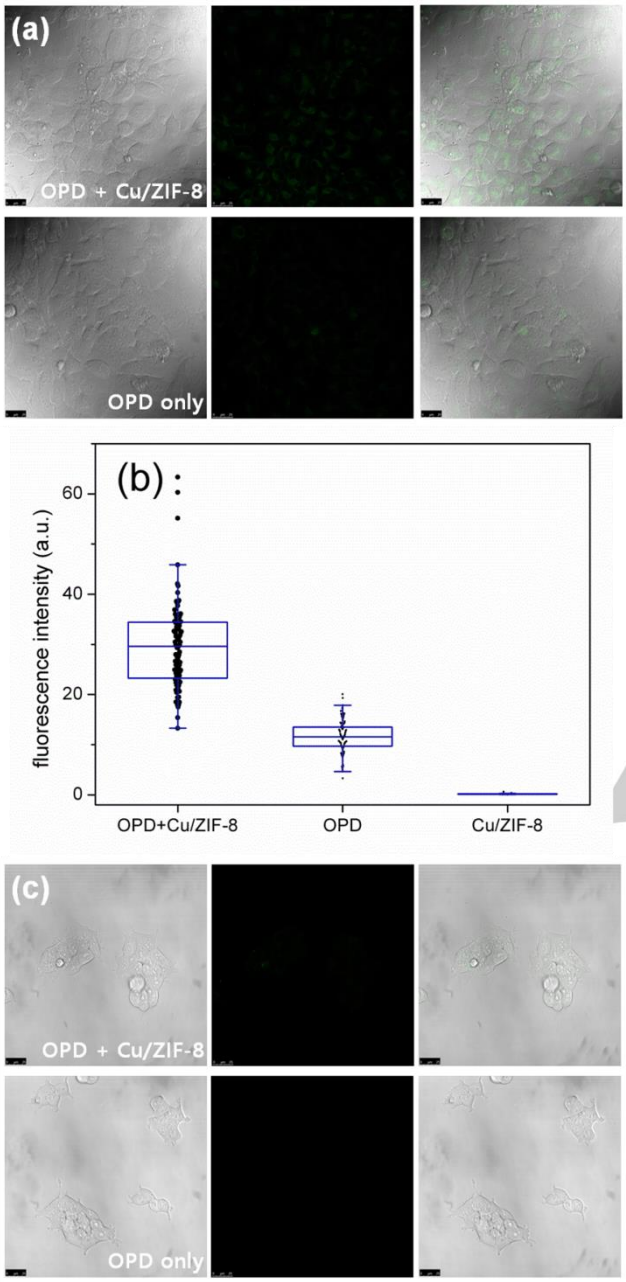

Figure 7. HeLa cell imaging using Cu/ZIF-8 and OPD. (a) Confocal microscopy images of the HeLa cells in the presence of both Cu/ZIF-8 and OPD (top) and OPD only (bottom) (scale bar = 25 μm). The images are optical, fluorescence, and merged microscopy images, from left to right. (b) Fluorescence intensity from the HeLa cells in the presence of Cu/ZIF-8 and/or OPD. Fluorescence intensity was measured from 100 randomly selected cells for each sample. (c) Confocal microscopy images of the HEK293T cells in the presence of both Cu/ZIF-8 and OPD (top) and OPD only (bottom) (scale bar = 25 μm).

To identify the ROS causing the OPD oxidation in a cell, tests were conducted using H_2O_2, •OH, $^1O_2$, and O_2^-, which are

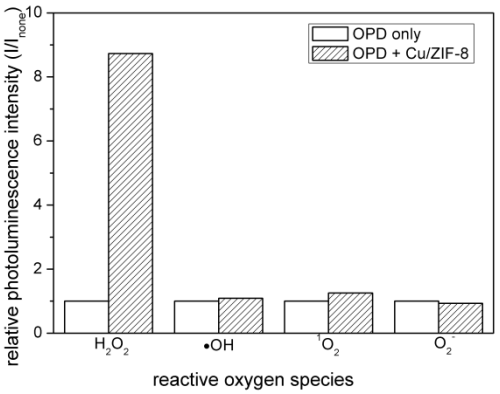

Figure 8. Photoluminescence emitted from the DAP (oxidized OPD) by various ROS in the presence/absence of Cu/ZIF-8 nanocrystals. I_{none} represents the intensity of the photoluminescence in the absence of Cu/ZIF-8 nanocrystals.

common ROS present in a cancer cell.[42] These ROS were prepared chemically or biologically (SI, methods for preparation of ROS) and subsequently reacted with OPD in the presence of Cu/ZIF-8. The photoluminescence (λ_{em} = 550 nm) intensity from DAP was monitored to identify the oxidation of OPD by the active ROS species. All ROS oxidized OPD, even in the absence of Cu/ZIF-8. However, remarkable oxidation of OPD showing outstanding photoluminescence occurred when H_2O_2 was applied in the presence of Cu/ZIF-8. By contrast, enhanced oxidation of OPD was hardly observable for the other ROS even in the presence of Cu/ZIF-8 (Figure 8). This result strongly supports that H_2O_2 is the key ROS in the HeLa cell that produces oxidative active species through the interaction with Cu/ZIF-8. The sensitivity of Cu/ZIF-8 nanocatalyst to H_2O_2 is comparable to other probes for fluorescence imaging of intracellular H_2O_2 such as hemin-decorated gold nanoparticle[46] and mesoporous silica nanoparticles decorated with ferrocene[47] or a cyanine-derivative.[48]

Conclusions

In summary, reaction kinetics and cancer cell imaging data demonstrated that the Cu/ZIF-8 nanocrystals could be used as an oxidative catalyst that has low toxicity. The Cu atoms doped in ZIF-8 working as active sites to oxidize an organic substance through selective interaction with H_2O_2, along with the stable ZIF-8 structure in the aqueous environment, were responsible for the high catalytic activity and reactivity with the ROS rich in a cancer cell. In comparison to other MOF-based oxidative catalysts requiring the heme cofactor for expression of the oxidative activity, this Cu/ZIF-8 could be prepared without other biological substances, which enabled facile preparation of the catalysts without complication. Furthermore, the considerable affinity to the substrates, including specificity to H_2O_2 among various ROS in a cell, could confirm the capability of Cu/ZIF-8

for imaging of HeLa cell. The catalytic activity and low toxicity of this easy-to-prepare Cu/ZIF-8 make this nanocrystal an appealing heterogeneous catalyst for microbiological analysis as well as conventional oxidative catalysis used in various chemical processes.

Experimental Section

Chemicals

The reagents for Cu/ZIF-8 synthesis were purchased from Sigma-Aldrich: zinc nitrate hexahydrate ($Zn(NO_3)_2{\cdot}6H_2O$, reagent grade, 98%), copper nitrate trihydrate ($Cu(NO_3)_2{\cdot}3H_2O$, puriss. p.a., 99-104%) and 2-methylimidazole (Hmim, 99%). In the catalysis experiments, *o*-phenylenediamin (OPD, 98%, Sigma) was used as a substrate. All chemicals were used as received.

Preparation of Cu/ZIF-8

To prepare Cu-doped ZIF-8, 35 mL of 2 M Hmim solution and 10 mL of metal precursor solution containing 180 mM $Zn(NO_3)_2$ and 20 mM $Cu(NO_3)_2$ were prepared. The metal precursor solution was mixed with the Hmim solution under vigorous stirring and aged 1 h. The final molar ratio of the synthesis solution was Zn:Cu:Hmim:water = 0.9:0.1:35:1280. After 1 h of stirring, the Cu/ZIF-8 crystals were precipitated and separated by centrifugation (9,000 rpm, 15 min). The remaining chemicals were washed off with deionized water three times. After vacuum drying for 12 h at 60 °C, beige coloured powder was obtained. Undoped ZIF-8 was synthesized through the same process without addition of $Cu(NO_3)_2$.

Characterization

The crystalline structure of the as-prepared Cu/ZIF-8 was characterized by an X-ray diffraction analyser (XRD, Ultima IV, Rigaku) equipped with a CuK_α radiation source (λ = 1.542 Å). XRD spectra of Cu/ZIF-8 and ZIF-8 were obtained over the ranges of 5° to 55° (step size: 0.02°, rate: 2°/min). For the characterization of surface area and pore volume, Brunauer–Emmett–Teller (BET) analyses on ZIF-8 and Cu/ZIF-8 were conducted. The dried powder samples were degassed at 150 °C in a vacuum for 3 h, and then N_2 adsorption/desorption isotherms were obtained using a surface-area and pore-size analyser (BET, Autosorb-iQ 2ST/MP, Quantachrome). The isotherms were analysed using the BET method and the pore volume was determined by the Horvath–Kawazoe equation. The microscopic image analysis and Cu ion characterization of Cu/ZIF-8 were performed by transmission electron microscopy (TEM, JEM-ARM 200F, JEOL, 200kV) equipped with EDX (Inca, Oxford, U.K.) and scanning electron microscopy (SEM, JSM-6701F, JEOL). To prepare the sample for TEM analysis, Cu/ZIF-8 powder was re-dispersed in H_2O and then dropped on the nickel grid. The nickel grid was used to identify the Cu in the Cu/ZIF-8. The content of Cu ions was examined from inductively coupled plasma mass spectrometry (ICP-MS, ICP-MS 7900, Agilent).

Catalytic oxidative activity of Cu/ZIF-8

The catalytic oxidative activity of Cu/ZIF-8 was evaluated from the oxidation of *o*-phenylenediamine (OPD), which is oxidized to 2,3-diaminophenazine (DAP), displaying a yellow colour. The colour change following the OPD oxidation was monitored using a UV−vis spectrophotometer (S-3100, Scinco, λ_{abs} = 420 nm) under mild stirring. Catalytic activity measurement was performed using 0.1 mL of Cu/ZIF-8 suspension (1 mg/mL) in a HEPES buffer (50 mM, pH 7.2) and 1.7 mL of OPD solution (10 mM) in the same HEPES buffer at various concentrations. The oxidation was initiated by dropping 0.2 mL of H_2O_2 solution to the mixture of Cu/ZIF-8 and OPD solutions. The reaction rate was determined from the slope of the OPD oxidation at the initial stage. The kinetics of the catalytic reaction were analysed based on the Michaelis–Menten equation while measuring the reaction rate with respect to the variation in the OPD and H_2O_2 concentrations. The kinetic parameters of the Michaelis–Menten equation were determined from the double-reciprocal plot.

Cell viability test and cell imaging

The human embryonic kidney cells (HEK-293T cells) and human cervical cancer cells (HeLa cells) were cultured in Dulbecco's modified Eagle's medium (DMEM)/F12 (1:1) supplemented with 10% fetal bovine serum (FBS), 1% penicillin, and streptomycin under 5% CO_2 at 37 °C. For the cell viability test, MTT (3-(4,5-dimethylthiazol-2-yl)-2,5-diphenyltetrazolium bromide) assay was conducted. Briefly, the HeLa cells were seeded on a 96-well plate (1×10^4 cells per well) in 100 μL of DMEM cell culture medium. After 24 h, the medium was changed with a fresh DMEM medium mixture containing the proper concentrations of OPD, Cu/ZIF, and H_2O_2, and then the cells were incubated for another 12 h. After that, the medium was washed with the DPBS buffer solution and was replaced with DMEM solution (80 μL) containing MTT solution (0.5 mg/mL) for another 4 h. The medium was removed, leaving 25 μL, and then 50 μL of DMSO was added to the remaining medium in order to dissolve the formazan. A sunrise microplate reader (Tecan, Austria) was used to record the absorbance intensity at 540 nm. The experiments were repeated at least three times. The cell viability (%) was determined as % viability [= (OD of treated cell - OD of blank)/(OD of untreated cell - OD of blank) × 100], where OD is the optical density.

For the imaging studies of HeLa and HEK-293T cells, the cells (1×10^5 cells per dish) were seeded on the cover glass in a 12-well plate and cultured for 1 day. The medium was then replaced with fresh DMEM containing OPD and/or Cu/ZIF-8 (0.42 mM and 30 μg/mL, respectively). All time-dependent experiments were performed by washing cells with DPBS before the observation. Confocal images were obtained using a laser-scanning confocal microscope system (Leica TCS SP5 AOBS/Tandem, Leica Microsystems, Germany) at Korea Basic Science Institute, Gwangju Center.

Toxicity test of copper released from Cu/ZIF-8

HeLa cell viability against the copper ion liberated from Cu/ZIF-8 was conducted with exposure of the cells to copper nitrate trihydrate solutions. In the same method as described above, HeLa cells were cultured in a DMEM medium mixture containing various concentrations of copper nitrate trihydrate for 12 h, and then the MTT assay was performed. To evaluate the quantity of released Cu ions from Cu/ZIF-8, ICP-MS analyses on the liberated copper ion were conducted. First, the content of Cu and Zn atoms in Cu/ZIF-8 nanocrystals were determined. Cu/ZIF-8 nanocrystals were dissolved in the mixture of concentrated HNO3 and H_2O_2 fully to a concentration of 1 mg/mL, and then the dissolved solution was analysed using inductively coupled plasma mass spectrometry (ICP-MS). To evaluate the amount of Cu and Zn liberated from the Cu/ZIF-8 in cytosol, 4 mg of Cu/ZIF-8 nanocrystals were incubated in 4 mL of pH-controlled phosphate buffer saline solutions at pH 7.4 and 5.0, respectively. After 12 h of incubation at 37 °C, the supernatants of the Cu/ZIF-8 solution were collected and the concentrations of the liberated metal ions were measured.

Acknowledgements

This work was supported by the Korean Research Foundation Grant funded by the Korean government (MOEHRD) (NRF-2014K2A1B8046967) and by the Human Resources Program in Energy Technology of the Korea Institute of Energy Technology Evaluation and Planning (KETEP), a granted financial resource from the Ministry of Trade, Industry & Energy, Republic of Korea (No. 20174010201640).

Keywords: zeolitic imidazolate framework • copper • catalyst • oxidation • imaging

[1] A. Phan, C. J. Doonan, F. J. Uribe-Romo, C. B. Knobler, M. O'Keeffe, O. M. Yaghi, *Acc. Chem. Res.* **2010**, *43*, 58-67.
[2] R. Banerjee, A. Phan, B. Wang, C. Knobler, H. Furukawa, M. O'Keeffe, O. M. Yaghi, *Science* **2008**, *319*, 939-943.
[3] H. Wu, W. Zhou, T. Yildirim, *J. Am. Chem. Soc.* **2007**, *129*, 5314-5315.
[4] H. Hayashi, A. P. Côté, H. Furukawa, M. O'Keeffe, O. M. Yaghi, *Nat. Mater.* **2007**, *6*, 501-506.
[5] H. Jiang, B. Liu, T. Akita, M. Haruta, H. Sakurai, Q. Xu, J. Am. Chem. Soc. **2009**, *2*, 11302-11303.
[6] C. Chizallet, S. Lazare, D. Bazer-bachi, F. Bonnier, E. Soyer, A. Quoineaud, N. Bats, *J. Am. Chem. Soc.* **2010**, 132, 12365-12377.
[7] G. Lu, J. T. Hupp, *J. Am. Chem. Soc.* **2010**, *132*, 7832-7833.
[8] Y. Pan, Y. Liu, G. Zeng, L. Zhao, Z. Lai, *Chem. Commun.* **2011**, *47*, 2071-2073.
[9] K. S. Park, Z. Ni, A. P. Côté, J. Y. Choi, R. Huang, J. Fernando, H. K. Chae, M. O. Keeffe, O. M. Yaghi, *Proc. Nat. Acad. Sci. USA* **2006**, 103, 10186-10191.
[10] Q. Bao, Y. Lou, T. Xing, J. Chen, *Inorg. Chem. Commun.* **2013**, *37*, 170-173.
[11] J. H. Park, S. H. Park, S. H. Jhung, *J. Korean Chem. Soc.* **2009**, *53*, 553-559.
[12] H. Y. Cho, J. Kim, S. N. Kim, W. S. Ahn, *Microporous Mesoporous Mater.* **2013**, *169*, 180-184.
[13] M. C. McCarthy, V. Varela-Guerrero, G. V. Barnett, H. K. Jeong, *Langmuir* **2010**, *26*, 14636-14641.
[14] J. Cravillon, R. Nayuk, S. Springer, A. Feldhoff, K. Huber, M. Wiebcke, *Chem. Mater.* **2011**, *23*, 2130-2141.
[15] J. Cravillon, C. A. Schröder, H. Bux, A. Rothkirch, J. Caro, M. Wiebcke, *CrystEngComm* **2012**, *14*, 492-498.
[16] D. M. Schubert, D. T. Natan, C. B. Knobler, *Inorg. Chim. Acta* **2009**, *362*, 4832-4836.
[17] A. Schejn, A. Aboulaich, L. Balan, V. Falk, J. Lalevée, G. Medjahdi, L. Aranda, K. Mozet, R. Schneider, *Catal. Sci. Technol.* **2015**, *5*, 1829-1839.
[18] H. Zhang, S. Hwang, M. Wang, Z. Feng, S. Karakalos, L. Luo, Z. Qiao, X. Xie, C. Wang, D. Su, Y. Shao, G. Wu, *J. Am. Chem. Soc.* **2017**, *139*, 14143-14149.
[19] I. B. Vasconcelos, T. G. da Silva, G. C. G. Militão, T. A. Soares, N. M. Rodrigues, M. O. Rodrigues, N. B. da Costa, R. O. Freire, S. A. Junior, *RSC Adv.* **2012**, *2*, 9437-9442.
[20] C.-Y. Sun, C. Qin, X.-L. Wang, G.-S. Yang, K.-Z. Shao, Y.-Q. Lan, Z.-M. Su, P. Huang, C.-G. Wang, E.-B. Wang, *Dalt. Trans.* **2012**, *41*, 6906-6909.
[21] J. Deng, K. Wang, M. Wang, P. Yu, L. Mao, *J. Am. Chem. Soc.* **2017**, *139*, 5877-5882.
[22] J. Zhuang, C. H. Kuo, L. Y. Chou, D. Y. Liu, E. Weerapana, C. K. Tsung, *ACS Nano* **2014**, *8*, 2812-2819.
[23] F.-X. Qin, S.-Y. Jia, F.-F. Wang, S.-H. Wu, J. Song, Y. Liu, *Catal. Sci. Technol.* **2013**, *3*, 2761-2768.
[24] R. W. Larsen, L. Wojtas, J. Perman, R. L. Musselman, M. J. Zaworotko, C. M. Vetromile, *J. Am. Chem. Soc.* **2011**, *133*, 10356-10359.
[25] F. Luo, Y. Lin, L. Zheng, X. Lin, Y. Chi, *ACS Appl. Mater. Interfaces* **2015**, *7*, 11322-11329.
[26] D. Li, S. Wu, F. Wang, S. Jia, Y. Liu, X. Han, L. Zhang, S. Zhang, Y. Wu, *Mater. Lett.* **2016**, *178*, 48-51.
[27] S. Gupta, S. Zhao, O. Ogoke, Y. Lin, H. Xu, G. Wu, *ChemSusChem* **2017**, *10*, 774-785.
[28] M. Jian, B. Liu, R. Liu, J. Qu, H. Wang, X. Zhang, *RSC Adv.* **2015**, *5*, 48433-48441.
[29] G. Ye, D. Zhang, X. Li, K. Leng, W. Zhang, J. Ma, Y. Sun, W. Xu, S. Ma, *ACS Appl. Mater. Interfaces* **2017**, *9*, 34937-34943.
[30] J. A. Hunt, M. Ahmed, C. A. Fierke, *Biochem.* **1999**, *38*, 9054-9058.
[31] H. Sigel, *Angew. Chemie, Int. Ed. English* **1969**, *8*, 167-177.
[32] M. Zhao, H.-B. Wang, L.-N. Ji, Z.-W. Mao, *Chem. Soc. Rev.* **2013**, *42*, 8360-8375.
[33] A. L. Abuhijleh, *Polyhedron* **1996**, *15*, 285-293.
[34] L. Gao, J. Zhuang, L. Nie, J. Zhang, Y. Zhang, N. Gu, T. Wang, J. Feng, D. Yang, S. Perrett, X. Yan, *Nat. Nanotechnol.* **2007**, *2*, 577-583.
[35] M.-C. Kim, S.-Y. Lee, *Nanoscale* **2015**, *7*, 17063-17070.
[36] X. Wang, K. Qu, B. Xu, J. Ren, X. Qu, *Nano Res.* **2011**, *4*, 908-920.
[37] X. Lv, J. Weng, *Sci. Rep.* **2013**, *3*, 3285.
[38] Z. Wang, X. Lv, J. Weng, *Carbon* **2013**, *62*, 51-60.
[39] B. Yu, Z. Jin, L. Deng, X. Xu, L. He, J. Wang, Y. Tian, H. Chen, *J. Food Sci. Technol.* **2010**, *47*, 67-72.
[40] P. Sudarsanam, A. Rangaswamy, B. M. Reddy, *RSC Adv.* **2014**, *4*, 46378-46382.
[41] M. Liu, H. Zhao, S. Chen, H. Yu, X. Quan, *ACS Nano* **2012**, *6*, 3142-3151.
[42] D. Trachootham, J. Alexandre, P. Huang, *Nat. Rev. Drug Discov.* **2009**, *8*, 579-591.
[43] S. S. Deshpande *Enzyme Immunoassays: From concept to product development*, Chapman & Hill, New York, **1996**, 169.
[44] C. Tamames-Tabar, D. Cunha, E. Imbuluzqueta, F. Ragon, C. Serre, M. J. Blanco-Prieto, P. Horcajada, *J. Mater. Chem. B* **2014**, *2*, 262-271.
[45] A. M. Studer, L. K. Limbach, L. Van Duc, F. Krumeich, E. K. Athanassiou, L. C. Gerber, H. Moch, W. J. Stark, *Toxicol. Lett.* **2010**, *197*, 169-174.
[46] L. Zhang, F. Ma, J. Lei, J. Liu, H. Ju, *Chem. Sci.*, **2017**, 8, 4833-4839.
[47] C. Liu, W. Chen, Z. Qing, J. Zheng, Y. Xiao, S. Yang, L. Wang, Y. Li, R. Yang, *Anal. Chem.*, **2016**, 88, 3998-4003.
[48] L. Yang, N. Li, W. Pan, Z. Yu, B. Tang, *Anal. Chem.*, **2015**, 87, 3678-3684.

Entry for the Table of Contents (Please choose one layout)

Layout 1:

FULL PAPER

Copper-doped zeolitic imidazolate framework-8 (Cu/ZIF-8) nanocrystal exhibiting oxidative catalytic activity was used as imaging agent for reactive oxygen species of cancer cell.

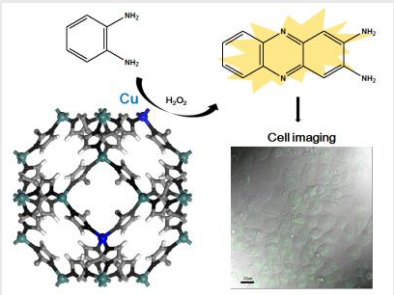

*Changjoon Keum, Sangwoo Park, Sang-Yup Lee**

Page No. – Page No.

Cancer-Cell Imaging Using Copper-Doped Zeolite Imidazole Framework-8 Nanocrystals Exhibiting Oxidative Catalytic Activity